

# Energetic stability and spatial inhomogeneity in the local electronic structure of relaxed twisted trilayer graphene

Xianqing Lin,<sup>1,\*</sup> Cheng Li,<sup>1</sup> Kelu Su,<sup>1</sup> and Jun Ni<sup>2</sup>

<sup>1</sup>College of Science, Zhejiang University of Technology, Hangzhou 310023, People's Republic of China

<sup>2</sup>State Key Laboratory of Low-Dimensional Quantum Physics and Frontier Science Center for Quantum Information, Department of Physics, Tsinghua University, Beijing 100084, People's Republic of China

(Dated: April 4, 2022)

We study the energetic stability and the local electronic structure of the general twisted trilayer graphene (TTG) with the top and bottom layers rotated with respect to the middle layer respectively by  $\theta$  and  $\theta'$ . Approximate supercells of the moiré-of-moiré superlattices with  $\theta$  and  $\theta'$  within  $1^\circ \sim 2^\circ$  are established to describe the structural and electronic properties of relaxed TTG with the periodic boundary condition. Full relaxation demonstrates that the commensurate TTG with  $\theta = \theta'$  has the local minimum total energy ( $E_{tol}$ ) at a fixed  $\theta$ , while  $E_{tol}$  first reaches a local maximum and begins to drop with decreasing  $\theta'$  for  $\theta' < \theta$ . Some regions exhibit enhanced in-plane relaxation in the top and bottom layers but suppressed relaxation in the middle layer and form a hexagonal network with the moiré-of-moiré length scale. The stacking configurations with the atoms in the three layers vertically aligned at the origin of the relaxed TTG supercells at  $\theta$  around  $1.6^\circ$  and  $\theta'$  around  $1.4^\circ$  have a high density of states (DOS) near the Fermi level ( $E_F$ ), which can reach that of the mirror symmetric TTG with equal twist angles of about  $1.7^\circ$ . In contrast, some other stackings can have rather low DOS around  $E_F$ . The significant stacking dependence of DOS for some TTG supercells demonstrates that the local electronic structure of TTG can exhibit strong spatial inhomogeneity when the twist angles are slightly away from those of the small supercells with large variations of DOS among different stackings. Moreover, the structural relaxation of TTG plays a crucial role in the high DOS and its strong stacking dependence.

## I. INTRODUCTION

The experimentally precise control of twist angles between consecutive layers in twisted trilayer graphene (TTG) has introduced superconductivity in TTG<sup>1-3</sup> beyond the magic-angle twisted bilayer graphene (TBG)<sup>4-12</sup>. In such superconducting TTG samples, the relative twist angle ( $\theta$ ) of the top layer and that ( $\theta'$ ) of the bottom layer with respect to the middle layer can share the same value of the magic angle ( $\theta_m$ ) around  $1.6^\circ$  with the mirror symmetry<sup>1,3</sup> or there is a small mismatch of about  $0.2^\circ$  between  $\theta$  and  $\theta'$  with their values still close to  $\theta_m$ <sup>2</sup>. The emergence of superconductivity in TTG implies a high density of states (DOS) around the Fermi level ( $E_F$ ), which has been confirmed by the theoretically calculated low-energy flat bands in TTG with  $\theta = \theta' = \theta_m$ <sup>13-25</sup>. However, the TTG with mismatched  $\theta$  and  $\theta'$  was predicted to host a rather low DOS at  $E_F$  when both  $\theta$  and  $\theta'$  lie in the window of  $1^\circ \sim 2^\circ$ <sup>26</sup>. It is noted that the rigid superlattices of TTG without relaxation were adopted to obtain such electronic properties<sup>26</sup>, while the structural reconstruction due to the superlattice relaxation may play a crucial role in enhancing the DOS of TTG with  $\theta \neq \theta'$ , similar to the mirror symmetric TTG<sup>15,22</sup> and magic-angle TBG<sup>27-34</sup>. Indeed, structural reconstruction has been observed experimentally in the general TTG with  $|\theta - \theta'|$  in the range of  $0.03^\circ \sim 0.25^\circ$ <sup>35</sup>. The peculiar reconstruction patterns were theoretical predicted for TTG and other twisted TMD trilayers<sup>36</sup>, while the energetic stability of TTG due to varying  $\theta$  and  $\theta'$  remains to be revealed. Therefore, it is crucial to account for the structural relaxation

to explore systematically the energetic stability and electronic structure of TTG with general  $\theta$  and  $\theta'$ .

In TTG with  $\theta \neq \theta'$ , the moiré-of-moiré superlattice with length scale of tens to hundreds of nanometers can arise with small  $|\theta - \theta'|$ <sup>36,37</sup>. Within such a large length scale, the local atomic structure represented by the local stackings between adjacent layers varies continuously. The structural relaxation can enhance the spacial variations of the local stacking configurations<sup>36</sup>. Then the local electronic structure, which can be characterized by the local DOS, may also exhibit strong spatial inhomogeneity, while previous theoretical investigations of TTG have focused on their global electronic properties<sup>14,26</sup>. In the trilayer heterostructures of TBG on the hexagonal boron nitride also with two twist angles<sup>38-44</sup>, the nonuniform spatial distributions of the local electronic and topological properties were demonstrated theoretically and can be described by the supermoiré picture<sup>43</sup>.

Here, full relaxation has been done for TTG supercells with general  $\theta$  and  $\theta'$  within  $1^\circ \sim 2^\circ$  to explore their energetic and electronic properties. We find that the commensurate TTG with  $\theta = \theta'$  has the local minimum total energy ( $E_{tol}$ ) at a fixed  $\theta$ , while  $E_{tol}$  first reaches a local maximum and begins to drop with decreasing  $\theta'$  for  $\theta' < \theta$ . The relaxed TTG with  $\theta$  around  $1.6^\circ$  and  $\theta'$  around  $1.4^\circ$  can have large DOS near  $E_F$  for some stacking configurations, and the TTG with these twist angles exhibits strong spatial inhomogeneity in the local electronic structure demonstrated by the stacking dependent DOS.

The outline of this paper is as follows: In Sec. II we present the structural configurations of TTG supercells.

The energetic stability and the in-plane structural deformation of fully relaxed TTG are shown in Sec. III. The stacking dependent electronic structure of relaxed TTG supercells and the spatial distribution of the local electronic structure in the completely incommensurate TTG are discussed in Sec. IV. Section V presents the summary and conclusions.

## II. SUPERCELLS OF THE GENERAL TTG

We first establish the approximate but accurate enough supercells of TTG, which are used to describe the energetic and electronic properties of the relaxed structures with the periodic boundary condition. In a TTG, the middle layer (G2) is fixed, and the top (G3) and bottom (G1) layers are rotated by  $\theta$  and  $\theta'$  counterclockwise, respectively, as seen in Fig. 1(a). The unit cell in G2 is spanned by the basis vectors  $\mathbf{a}_1 = a(\sqrt{3}/2, -1/2)$  and  $\mathbf{a}_2 = a(\sqrt{3}/2, 1/2)$ , where  $a = 2.46$  Å is the lattice constant of graphene. Double moiré superlattices arise between adjacent layers. Approximate periodic supercells can be built for such double superlattices. The supercells are taken to be strictly periodic for the superlattice between G3 and G2 (G3/G2) and are spanned by  $\mathbf{L}_1 = N\mathbf{a}_1 + (N+r)\mathbf{a}_2$  and  $\mathbf{L}_2 = T_{60^\circ}\mathbf{L}_1$  with  $N$  and  $r$  positive integers and  $T_{60^\circ}$  the rotation operator by  $60^\circ$ <sup>45–48</sup>. The twist angle  $\theta$  is given by  $\tan(\theta/2) = r/[\sqrt{3}(2n+r)]$  and the length ( $L$ ) of  $\mathbf{L}_1$  can be expressed as  $L = ra/[2\sin(\theta/2)]$ . The supercell contains  $r \times r$  approximate moiré cells of G3/G2 as

$$(I - T_{-\theta})\mathbf{L}_1 = r(\mathbf{a}_2 - \mathbf{a}_1). \quad (1)$$

We find that  $\mathbf{L}_1$  cannot be an exact lattice vector of G1 when  $\theta' \neq \theta$ . However, a very slight biaxial strain ( $\epsilon$ ) in G1 can be introduced to make the supercell also strictly periodic in G1. Then a position  $\mathbf{r}$  in G2 is transformed to  $S\mathbf{r}$  in G1 with  $S = T_{\theta'}/(1 + \epsilon)$ . The supercell is taken to consist of  $(r+i) \times (r+i)$  approximate moiré cells between G2 and G1 (G2/G1) with

$$(S^{-1} - I)\mathbf{L}_1 = (r+i)(\mathbf{a}_1 - \mathbf{a}_2), \quad (2)$$

where  $i$  are small integers.  $\theta'$  and  $\epsilon$  can be solved from this equation. We consider systems with  $|\epsilon| < 10^{-4}$ , which requires  $i$  to be small integers. Then  $\theta'$  is expressed approximately as

$$\sin \theta' \simeq \frac{\sqrt{3}(i+r)(2N+r)}{2L^2}. \quad (3)$$

Zero and positive  $i$  give  $\theta' \geq \theta$  and a negative  $i$  gives  $\theta' < \theta$ . The structural parameters of each supercell are thus determined by the three integers  $N$ ,  $r$ , and  $i$ . The possible pairs of  $\theta'$  and  $\theta$  around  $1.65^\circ$  for supercells with  $N \leq 600$  ( $L \leq 262$  nm) are plotted in Fig. 1(b). The points in Fig. 1(b) form a large number of straight line segments. Each segment generally has the same  $i$ , and

$N$  and  $r$  vary within the segment, with the largest  $N$  and  $r$  occurring at the end toward small  $|\theta' - \theta|$ . There exist some series of supercell configurations with varying  $\theta'$  but the same  $\theta$ . The possible  $L$  oscillates with  $\theta'$  at the same  $\theta$ , as shown in Fig. 1(c) for  $\theta = 1.696^\circ$ , where each line has the same  $i$ . In addition, the reciprocal space of the TTG supercell is shown schematically in Fig. S1 of the SM.

The structural patterns in TTG can be considered as the moiré superlattices of the approximate moiré cells in G3/G2 and those in G2/G1. A strictly periodic supercell of TTG contains  $r \times r$  moiré cells in G3/G2 and  $(r+i) \times (r+i)$  moiré cells in G2/G1. Then there are  $|i| \times |i|$  approximate moiré-of-moiré cells within a periodic supercell for large  $r$  and small  $i$ .

Besides the supercell geometry, the stacking between the double moiré superlattices can also influence the energetic and electronic properties of TTG. The sublattice-A and sublattice-B atoms in a graphene unit cell are located at  $(\mathbf{a}_1 + \mathbf{a}_2)/3$  and  $2(\mathbf{a}_1 + \mathbf{a}_2)/3$ , respectively. In a moiré superlattice, the local stacking between adjacent layers varies continuously and can be characterized by the local in-plane relative shift vectors. At the origin, the local stacking between G3 and G2 is fixed to be the AA stacking, and the stacking arrangement of a supercell is determined by the local stacking between G2 and G1 at the origin and thus the corresponding shift vector ( $\tau_{21}$ ), as shown in Fig. S2 of the SM. At an in-plane position  $\mathbf{r}$ , the local shift vector between G2 and G1 can be taken as  $\delta' = (S^{-1} - I)\mathbf{r} + \tau_{21}$ . In a TTG with twist angles slightly away from those of the small supercells, the structure becomes completely incommensurate and can be described by the supermoiré picture<sup>43</sup>. In such incommensurate systems, the moiré superlattices in G3/G2 can still be taken to be periodic with cell vectors of  $\mathbf{L}_1$  and  $\mathbf{L}_2$ , while they are no longer lattice vectors in G1. When the position with AA stacking between G3 and G2 and also between G2 and G1 is chosen as the origin, the  $\delta'$  at  $\mathbf{L} = i_1\mathbf{L}_1 + i_2\mathbf{L}_2$  ( $i_1$  and  $i_2$  are integers) varies slowly with  $\mathbf{L}$ . For example, the supercell with  $N = 95$ ,  $r = 5$ , and  $i = -1$  has  $\theta = 1.696^\circ$  and  $\theta' = 1.357^\circ$ . For a TTG with the same  $\theta$  but  $\theta'$  smaller than that of this supercell by just  $0.01^\circ$ , the spatially varying  $\delta'$  at  $\mathbf{L}$  can be seen in Fig. 1(d). The  $\delta'$  can take any vector in a Wigner-Seitz cell of graphene for a TTG sample with dimensions of about  $1 \mu\text{m}$ . Then the local electronic properties around the position  $\mathbf{L}$  can be approximately characterized by the supercell with  $\tau_{21}$  equal to the  $\delta'$  at  $\mathbf{L}$ .

## III. STRUCTURAL RELAXATION OF TTG

Since the AB- and BA-like stackings between adjacent graphene layers are energetically favorable compared with other stackings<sup>27–32,34,36,49–66</sup>, spontaneous in-plane relaxation occurs in the rigid TTG due to the energy gain from the larger domains of energetically favorable local AB- and BA-like stackings. We have employed the con-

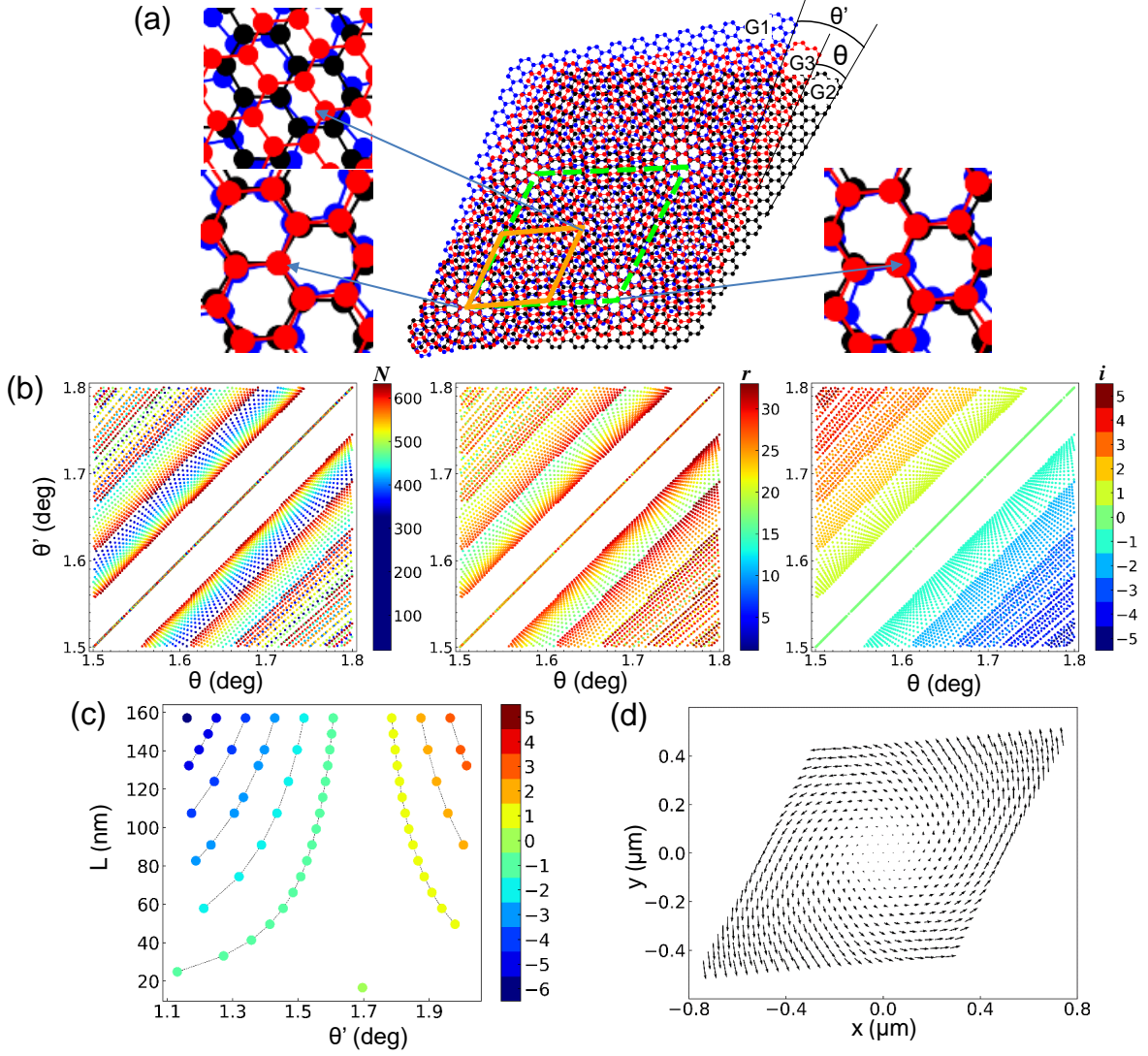


FIG. 1. (Color online) The geometry of the moiré-of-moiré superlattices in TTG. (a) The schematic view of the TTG with the top (G3) and bottom (G1) layers rotated respectively by  $\theta$  and  $\theta'$  counterclockwise with respect to the middle layer (G2). A moiré cell between G1 and G2 is represented by the solid lines and that between G2 and G3 is denoted by the dashed lines. The local stackings at some positions of the superlattices are shown in the insets. At the origin, the sublattice-A atoms in the three layers are exactly vertically aligned. When G1 is horizontally shifted, the local shift vector between G2 and G1 at the origin is denoted by  $\tau_{21}$ , so  $\tau_{21} = 0$  for this configuration. The configurations with different  $\tau_{21}$  can be seen in Fig. S1 of the Supplemental Material (SM). At other corners of the moiré cells, only the sublattice-A atoms in two layers are aligned, while a strictly periodic supercell consisting of these moiré cells can be constructed with G1 very slightly strained. (b) The three integers  $N$ ,  $r$ , and  $i$  determining the supercell geometry. The supercell size is proportional to  $N$ , and a supercell consists of  $r \times r$  moiré cells in G3/G2 and  $(r + i) \times (r + i)$  moiré cells in G2/G1. (c) The length ( $L$ ) of the supercell basis vectors as a function of  $\theta'$  at  $\theta = 1.696^\circ$ . (d) The spatially varying  $\delta'$  for TTG with  $\theta = 1.696^\circ$  and  $\theta' = 1.347^\circ$  at the lattice vectors  $\mathbf{L}$  of the small supercell with  $\theta = 1.696^\circ$  and  $\theta' = 1.357^\circ$ .

tinuum elastic theory to model the in-plane relaxation in the large TTG supercells, as detailed in the SM. The displacement field in each layer is expanded in Fourier series to solve the Euler-Lagrange equations, which minimize the total energy ( $E_{tot}$ ) of a supercell as a functional of the displacement fields. It is noted that the reciprocal lattice vectors of the supercell with large Fourier com-

ponents of the displacement fields are approximately the sum of the small reciprocal lattice vectors of the moiré cells in G2/G1 and those for G3/G2.

For the fully relaxed TTG, the  $E_{tot}$  as a function of  $\theta$  and  $\theta'$  is displayed in Fig. 2, where  $\theta$  is taken to be around the experimentally realized value of  $1.58^\circ$  and  $\theta'$  varies from about  $1.0^\circ$  to  $2.0^\circ$ . We find that the commen-



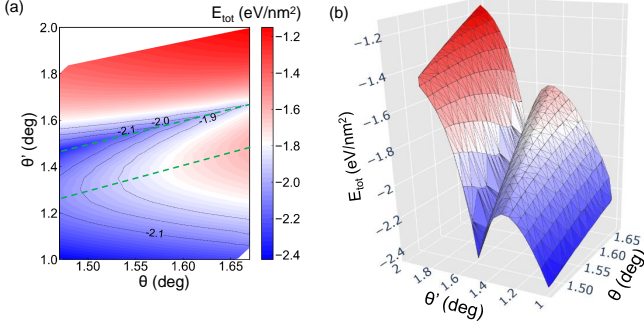


FIG. 2. (Color online) The total energy ( $E_{tot}$ ) of the relaxed TTG as a function of  $\theta$  and  $\theta'$ . (a, b) The contour plot and the 3D view of the  $E_{tot}$  map. The green dashed lines in (a) denote systems with  $\theta = \theta'$  and those with the local maximum of  $E_{tot}$  at a fixed  $\theta$ .

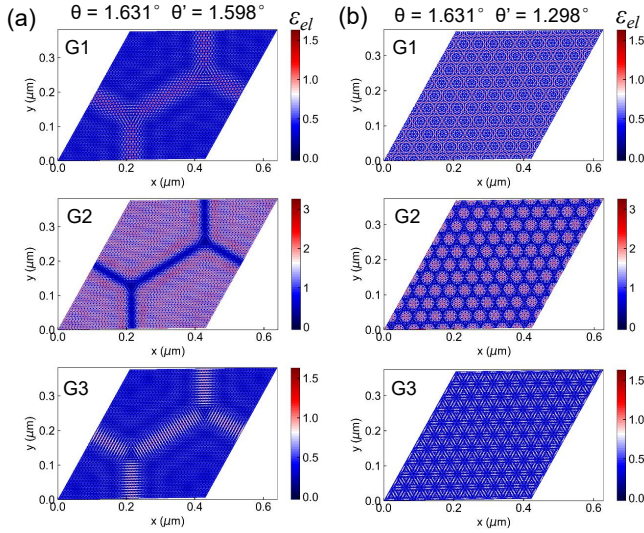


FIG. 3. (Color online) The spatial distribution of the elastic energy density ( $\varepsilon_{el}$ ) in each layer for a supercell of TTG with  $\theta = 1.631^\circ$  and  $\theta' = 1.598^\circ$  ( $N = 989$ ,  $r = 50$ ,  $i = -1$ ) and that with  $\theta = 1.631^\circ$  and  $\theta' = 1.298^\circ$  ( $N = 969$ ,  $r = 49$ ,  $i = -10$ ).  $\varepsilon_{el}$  is in the unit of meV per graphene unit cell.

surate TTG with  $\theta' = \theta$  indeed has the local minimum energy at a fixed  $\theta$ . For  $\theta' > \theta$ ,  $E_{tot}$  grows fast with increasing  $\theta'$ . In contrast,  $E_{tot}$  first reaches a local maximum and then declines with decreasing  $\theta'$  for  $\theta' < \theta$ . So the TTG with  $\theta'$  slightly away from  $\theta$  may undergo spontaneous structural transformation to reach the commensurate configuration with equal twist angles, while the TTG with  $\theta'$  rather below  $\theta$  can maintain the relative difference between the twist angles. The appearance of  $E_{tot}$  local maximums at  $\theta' < \theta$  can be attributed to the competition between the constructive relaxation in the middle layer G2 at  $\theta' = \theta$  and the stronger relaxation in G1 for smaller  $\theta'$  with larger moiré superlattices

in G2/G1. At  $\theta' = \theta$ , the energy favorable AB- or BA-like stackings in G2/G1 and those in G3/G2 are at the same positions, so the relaxation in G2 can be greatly enhanced due to such constructive interference of the local stackings in the double superlattices. The constructive relaxation becomes weak for the large  $\theta$  with a small commensurate supercell. Then the  $\theta'$  at the  $E_{tot}$  local maximum increases with  $\theta$ .

In the moiré-of-moiré superlattices of TTG, the local stackings exhibit different approximate spatial periods. In the long period, the in-plane structural relaxation can show strong spatial inhomogeneity, especially for configurations with small  $|i|$  at  $\theta'$  close to  $\theta$ , as shown in Fig. 3. Most regions in the G2 layer have much larger in-plane strain than that in G1 and G3, while some continuous positions forming a hexagonal network have greatly suppressed relaxation in G2 but enhanced relaxation in G1 and G3. Such hexagonal networks are just the  $|i| \times |i|$  approximate moiré-of-moiré superlattices in a supercell, as clearly demonstrated for  $|i| = 1$  in Fig. 3(a) and for  $|i| = 10$  in Fig. 3(b). For small  $|i|$ , the hexagonal networks with large strain in G1 and G3 can be considered as domains walls separating regions with relatively small structural deformation. Such domains walls may be observed through the flexoelectric effect similar to that in other twisted graphene layers<sup>67,68</sup>. In addition,  $\tau_{21} = \mathbf{0}$  is adopted to produce the strain maps, so the atoms in the three layers are approximately aligned at the center of each domain.

#### IV. ELECTRONIC STRUCTURE OF RELAXED TTG

For a relaxed TTG supercell with given  $\theta'$ ,  $\theta$ , and  $\tau_{21}$ , the band structure and the density of states can be obtained from the tight-binding Hamiltonian, which is diagonalized in the plane-wave-like basis functions as detailed in the SM. In the following, the size of each TTG supercell is labeled by the  $r \times r$  moiré cells of G3/G2 in it. We first consider configurations with a fixed  $\theta = 1.696^\circ$  but varying  $\theta'$  and  $\tau_{21}$ . Figure 4 displays their DOS for the three  $\tau_{21}$  of  $\tau_g = \mathbf{0}$ ,  $\tau_m = -\mathbf{a}_1/2$ , and  $\tau_k = -(\mathbf{a}_1 + \mathbf{a}_2)/3$  and four increasing  $\theta'$ . The maximum DOS (mDOS) around  $E_F$  for  $\tau_g$  can reach values higher than  $12 \text{ nm}^{-2} \text{ eV}^{-1}$  for  $\theta'$  around  $1.357^\circ$  with a single DOS peak at  $E_F$ . These mDOS are as high as that of the mirror symmetric TTG at  $\theta' = \theta = 1.696^\circ$ , as shown in Fig. 4(a). The mDOS for  $\tau_g$  increases with  $\theta'$  from  $1.1^\circ$  to about  $1.4^\circ$ , and it tends to become lower for larger  $\theta'$  except for  $\theta'$  just equal to  $\theta$ . The single DOS peak at  $E_F$  begins to be split for  $\theta' \geq 1.5^\circ$ . In contrast, the mDOSs for  $\tau_m$  and  $\tau_k$  have much smaller values than that for  $\tau_g$  at  $\theta'$  from about  $1.3^\circ$  to  $\theta$ , and they just change slightly with  $\theta'$ . For  $\theta' > \theta$ , the mDOSs for the three stacking configurations have similar values, suggesting that the electronic structure of such TTG is approximately independent of the stacking  $\tau_{21}$  so that

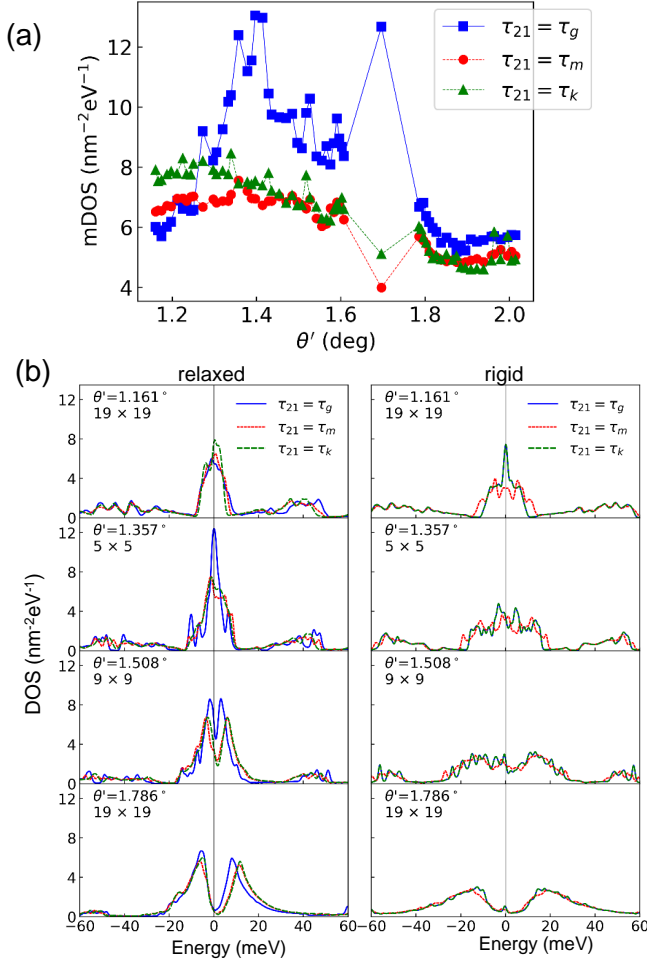


FIG. 4. (Color online) (a) The mDOS for the three stacking configurations with  $\tau_{21}$  of  $\tau_g$ ,  $\tau_k$ , and  $\tau_m$  as a function of  $\theta'$  at  $\theta = 1.696^\circ$ . (b) The DOS for the relaxed and rigid TGT supercells with different  $\theta'$  and stackings at  $\theta = 1.696^\circ$ . The size of the supercell containing  $r \times r$  moiré cells of G3/G2 is labeled by  $r \times r$ .

their electronic properties are almost spatially uniform for systems with twist angles slightly away from those of the supercells. We note that the mDOS can be significantly underestimated without the in-plane structural relaxation for all the three stacking configurations, as shown in Fig. 4(b). At  $\theta'$  around  $1.36^\circ$  or larger than that, the mDOS for  $\tau_g$  is just about  $4 \text{ nm}^{-2}\text{eV}^{-1}$  without relaxation, which is only one third of that for the relaxed system at  $\theta' = 1.357^\circ$ . This demonstrates that the electronic structure of TGT around  $E_F$  is sensitive to the in-plane structural deformation due to the relaxation, which can enhance the high DOS around  $E_F$ . In addition, the unrelaxed structures with  $\tau_g$  and  $\tau_k$  have the same DOS, while the DOS for  $\tau_m$  is different due to the broken  $C_{3z}$  symmetry. For a small  $\theta'$  of  $1.161^\circ$ , the mDOS without relaxation reaches a rather high value for  $\tau_g$ . Such a high mDOS for unrelaxed structures with a

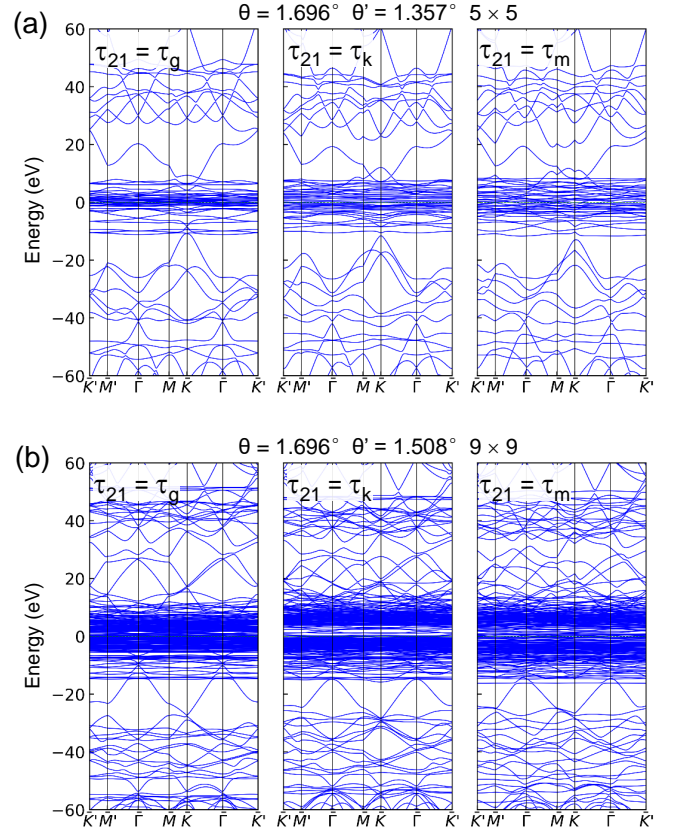


FIG. 5. (Color online) The band structures of the three stackings of the  $5 \times 5$  TGT supercell at  $\theta = 1.696^\circ$  and  $\theta' = 1.357^\circ$  (a) and those of the  $9 \times 9$  supercell at  $\theta = 1.696^\circ$  and  $\theta' = 1.508^\circ$  (b).

small  $\theta'$  around  $1.1^\circ$  but a large  $\theta$  is consistent with the previous study of the rigid TGT<sup>26</sup>.

The large DOS around  $E_F$  in relaxed TGT is also reflected by the band structures of the supercells, as shown in Fig. 5. For a supercell consisting of a rather large number of moiré cells in G3/G2 or G2/G1, most subbands around  $E_F$  become almost dispersionless. For the  $5 \times 5$  supercell at  $\theta' = 1.357^\circ$  and  $\theta = 1.696^\circ$ , such subbands lie in an energy range of about 20 meV around  $E_F$  with the  $\tau_g$  configuration having flat subbands just at  $E_F$  and thus the largest mDOS. For  $\theta' = 1.508^\circ$  and  $\theta = 1.696^\circ$  with a larger  $9 \times 9$  supercell, the flat subbands appear in a larger energy range, and there are fewer subbands at  $E_F$  than some other energies close to  $E_F$ , leading to the split DOS peaks seen in Fig. 4(b). At energies quite away from  $E_F$  by about 40 meV, there are also satellite flat subbands embedded in the dispersive bands, giving rise to the small DOS peaks away from  $E_F$ . In addition, the band structures show that most subbands around  $E_F$  connect or cross other bands, while some bands are separated from nearby bands by direct gaps smaller than 1 meV, as seen in Fig. 5(a) for the  $\tau_k$  and  $\tau_m$  configurations around the  $K$  point. Such small direct gaps are

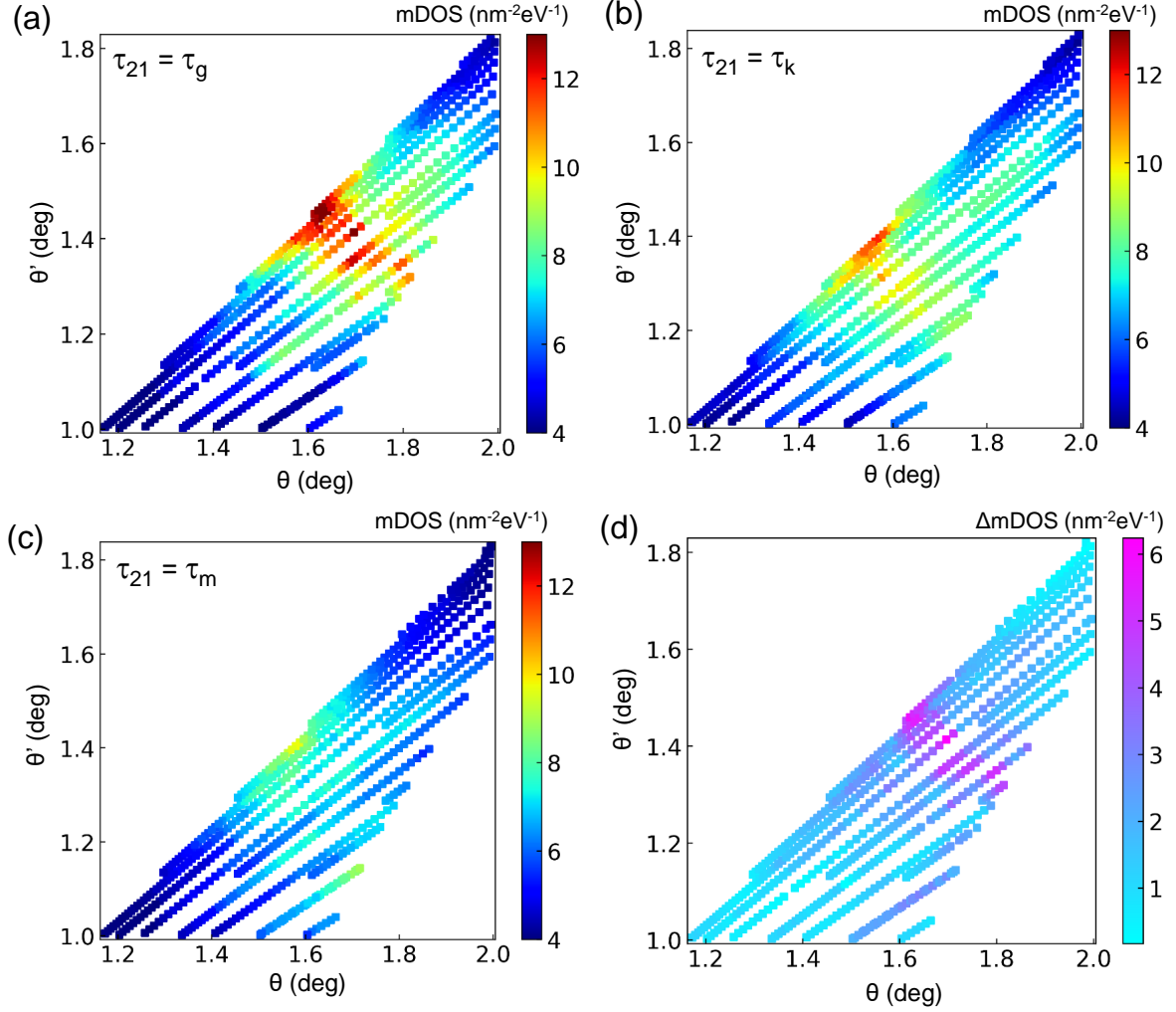


FIG. 6. (Color online) (a,b,c) The mDOS maps as functions of  $\theta$  and  $\theta'$  ( $\theta > \theta'$ ) for the three stackings. The mDOS of the configurations with  $L$  smaller than about 90 nm are shown. (d) The map of the largest difference of mDOS ( $\Delta\text{mDOS}$ ) among the three stackings.

present in both relaxed and rigid supercells and are thus caused by the small approximate supercell. When the supercell becomes large, the direct gaps tend to vanish, as shown in Fig. 5(b), and the systems become perfect metal, consistent with the previous calculations of the rigid TTG<sup>14</sup>.

The occurrence of high mDOS and the  $\theta'$  with the highest mDOS depend on the value of  $\theta$ . Figure 6 illustrates the mDOS maps as functions of  $\theta$  and  $\theta'$  ( $\theta \geq \theta'$ ) for supercells with  $L \leq 100$  nm for the three  $\tau_{21}$ . The configuration with  $\theta \leq \theta'$  has the same DOS as that of the corresponding system with  $\theta \geq \theta'$ . For supercells with  $\tau_g$ , mDOS can reach  $10 \text{ nm}^{-2}\text{eV}^{-1}$  for  $\theta$  in the range of about  $1.5^\circ \sim 1.8^\circ$ , and the  $\theta'$  with the highest mDOS decreases with  $\theta$  and lies in the range of about  $1.3^\circ \sim 1.5^\circ$ . For  $\theta$  and  $\theta'$  beyond these ranges, the mDOS is rather low. The highest mDOS of the supercells with  $\tau_k$  and  $\tau_m$  is smaller than that with  $\tau_g$ . All the mDOS for  $\tau_m$  are

lower than  $10 \text{ nm}^{-2}\text{eV}^{-1}$ , indicating that the DOS for  $\tau_m$  is weakly related to  $\theta$  and  $\theta'$ . For the configurations of  $\theta$  and  $\theta'$  with high mDOS at  $\tau_{21} = \tau_g$ , the differences of mDOS among the three stackings are large, as shown in Fig. 6(d), implying that the electronic structure of these twist configurations of TTG can be rather spatially inhomogeneous when the twist angles are slightly away from those of the small supercells.

For the  $5 \times 5$  supercell at  $\theta = 1.696^\circ$  and  $\theta' = 1.357^\circ$ , we have systematically calculated the variation of mDOS with all possible stackings, as shown in Fig. 7(a). The mDOS maintains high values in a rather large region with  $|\tau_{21}|$  smaller than about  $0.5 \text{ \AA}$ , while it drops fast for large  $|\tau_{21}|$ . The configurations around  $\tau_m$  have the smallest mDOS. In a TTG with twist angles slightly away from those of such small commensurate supercells, the structural configurations in different positions can take various stackings and thus exhibit distinct local electronic struc-

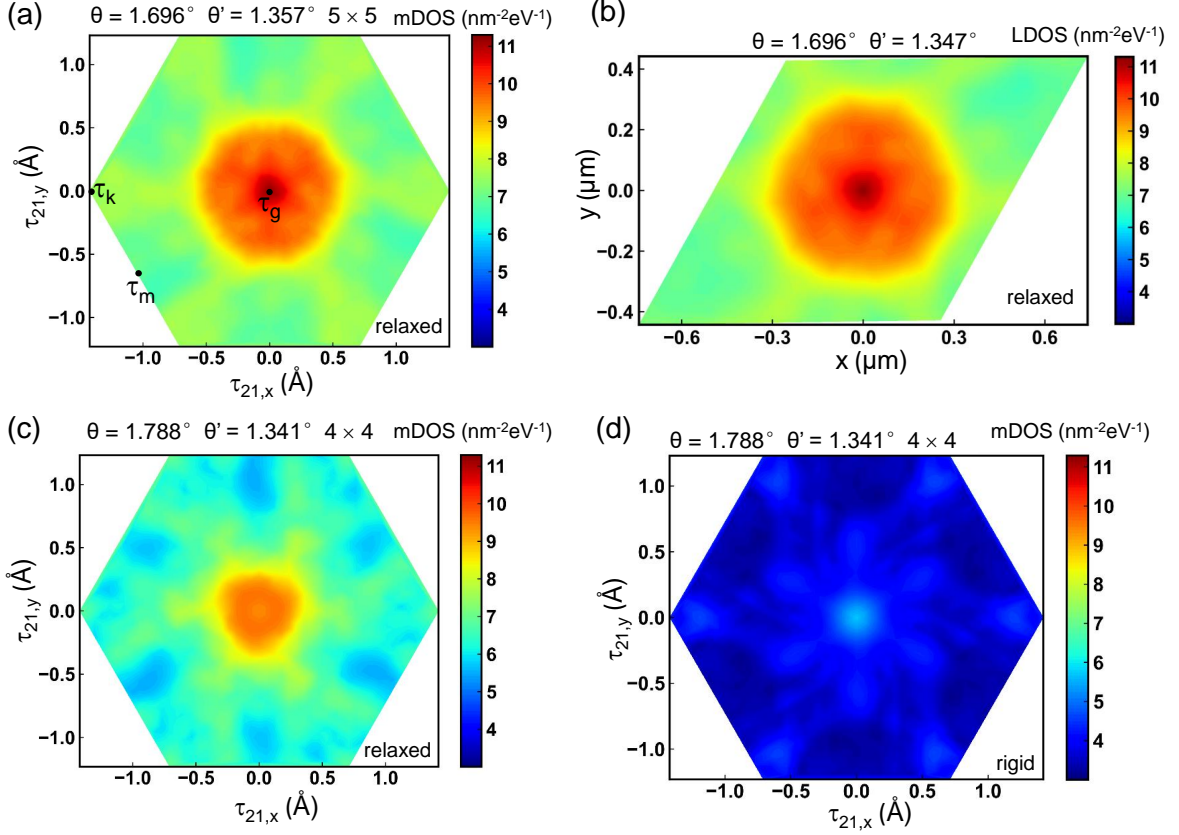


FIG. 7. (Color online) The mDOS maps as functions of all the possible stacking  $\tau_{21}$  in the Wigner-Seitz cell of graphene for the relaxed  $5 \times 5$  supercell at  $\theta = 1.696^\circ$  and  $\theta' = 1.357^\circ$  (a), and the relaxed (c) and rigid (d)  $4 \times 4$  supercell at  $\theta = 1.696^\circ$  and  $\theta' = 1.357^\circ$ . The positions of  $\tau_g$ ,  $\tau_k$ , and  $\tau_m$  are labeled in (a). (b) The spatial map of the local mDOS for the TTG with  $\theta = 1.696^\circ$  but  $\theta'$  smaller than  $1.357^\circ$  by just  $0.01^\circ$ .

tures. The electronic properties of the incommensurate systems can be described by the supermoiré picture. The local DOS at a position  $\mathbf{r}$  is taken approximately as that of the small supercell with the stacking  $\tau_{21}$  at  $\mathbf{r}$ . Figure 7(b) exhibits the spatial map of the local DOS for the TTG with  $\theta = 1.696^\circ$  but  $\theta'$  smaller than  $1.357^\circ$  by just  $0.01^\circ$ . The spatial variation of the local stacking  $\tau_{21}$  in this TTG has been shown in Fig. 1(d). The mDOS has large values in positions  $\mathbf{r}$  around the origin with zero  $|\tau_{21}|$  for  $|\mathbf{r}|$  smaller than about  $0.3 \mu\text{m}$ , and it becomes rather small in other positions, indicating that the local electronic structure is strongly inhomogeneous for this configuration. Other incommensurate configurations around the small supercells with large variations of mDOS with  $\tau_{21}$  [see Fig. 6(d)] can also exhibit inhomogeneous distribution of the local electronic properties, while the dimension of the region with high mDOS depends on the twist angles. The  $4 \times 4$  supercell at  $\theta = 1.788^\circ$  and  $\theta' = 1.341^\circ$  has a smaller region of  $\tau_{21}$  with high mDOS, as shown in Fig. 7(c). Calculations show that the size of the high-mDOS region is roughly proportional to the mDOS with  $\tau_g$ . It is noted that such spatial inhomogeneity in the local electronic structure can only be observed

with the in-plane structural relaxation. The mDOS of unrelaxed structures remain small for all possible  $\tau_{21}$ , as shown in Fig. 7(d).

## V. SUMMARY AND CONCLUSIONS

Supercells of the general TTG with twist angles  $\theta$  and  $\theta'$  within  $1^\circ \sim 2^\circ$  have been constructed to perform the full structural relaxation of TTG and obtain the electronic structure of the relaxed TTG with the periodic boundary condition. A supercell contains  $|i| \times |j|$  approximate moiré-of-moiré cells with  $i$  a small integer, and its stacking configurations are characterized by the local in-plane shift vector  $\tau_{21}$  between G2 and G1 at the origin with the AA stacking between G3 and G2. The in-plane relaxation of large TTG supercells is performed employing the continuum elastic theory by solving the Euler-Lagrange equations, where the displacement field in each layer is expanded in Fourier series. It is shown that the supercell reciprocal lattice vectors with large Fourier components are approximately the sum of the small reciprocal lattice vectors of the moiré cells in G2/G1 and



those for G3/G2. We find that the commensurate TTG with  $\theta = \theta'$  has the local minimum total energy ( $E_{tol}$ ) at a fixed  $\theta$ , while  $E_{tol}$  first reaches a local maximum and begins to drop with decreasing  $\theta'$  for  $\theta' < \theta$ . Some regions exhibit enhanced in-plane relaxation in the top and bottom layers but suppressed relaxation in the middle layer and form a hexagonal network with the moiré-of-moiré length scale.

The band structure and the density of states of a relaxed TTG supercell are obtained by diagonalizing the Hamiltonian in the plane-wave-like basis functions. The TTG supercells with the  $\tau_g$  stacking have high mDOS at  $\theta$  around  $1.6^\circ$  and  $\theta'$  around  $1.4^\circ$ , which can reach that of the mirror symmetric TTG with equal twist angles of about  $1.7^\circ$ . In contrast, the configurations with the  $\tau_k$  and  $\tau_m$  stackings can have rather low mDOS. Systematic calculations of the variations of mDOS with all possible stackings demonstrate the significant stacking dependence of the mDOS for some TTG supercells. The

supermoiré calculations show that the local electronic structure of TTG can exhibit strong spatial inhomogeneity when the twist angles are slightly away from those of the small supercells with large variations of DOS among different stackings. Moreover, the structural relaxation of TTG plays a crucial role in the high local DOS and their strong stacking dependence as the mDOS of unrelaxed structures remain small for all possible stackings.

## ACKNOWLEDGMENTS

We gratefully acknowledge valuable discussions with D. Tománek, H. Xiong, and S. Yin. This research was supported by the National Natural Science Foundation of China (Grants No. 11974312 and No. 11774195) and the Open Research Fund of CNMGE Platform & NSCC-TJ.

---

\* E-mail: [xqlin@zjut.edu.cn](mailto:xqlin@zjut.edu.cn)

- <sup>1</sup> J. M. Park, Y. Cao, K. Watanabe, T. Taniguchi, and P. Jarillo-Herrero, "Tunable strongly coupled superconductivity in magic-angle twisted trilayer graphene," *Nature* **590**, 249 (2021).
- <sup>2</sup> Z. Hao, A. M. Zimmerman, P. Ledwith, E. Khalaf, D. H. Najafabadi, K. Watanabe, T. Taniguchi, A. Vishwanath, and P. Kim, "Electric field-tunable superconductivity in alternating-twist magic-angle trilayer graphene," *Science* **371**, 1133 (2021).
- <sup>3</sup> Y. Cao, J. M. Park, K. Watanabe, T. Taniguchi, and P. Jarillo-Herrero, "Pauli-limit violation and re-entrant superconductivity in moiré graphene," *Nature* **595**, 526 (2021).
- <sup>4</sup> R. Bistritzer and A. H. MacDonald, "Moiré bands in twisted double-layer graphene," *Proc. Natl. Acad. Sci. U.S.A.* **108**, 12233 (2011).
- <sup>5</sup> Y. Cao, V. Fatemi, A. Demir, S. Fang, S. L. Tomarken, J. Y. Luo, J. D. Sanchez-Yamagishi, K. Watanabe, T. Taniguchi, E. Kaxiras, R. C. Ashoori, and P. Jarillo-Herrero, "Correlated insulator behaviour at half-filling in magic-angle graphene superlattices," *Nature* **556**, 80 (2018).
- <sup>6</sup> Y. Cao, V. Fatemi, S. Fang, K. Watanabe, T. Taniguchi, E. Kaxiras, and P. Jarillo-Herrero, "Unconventional superconductivity in magic-angle graphene superlattices," *Nature* **556**, 43 (2018).
- <sup>7</sup> X. Lu, P. Stepanov, W. Yang, M. Xie, M. A. Aamir, I. Das, C. Urgell, K. Watanabe, T. Taniguchi, G. Zhang, A. Bachtold, A. H. MacDonald, and D. K. Efetov, "Superconductors, orbital magnets and correlated states in magic-angle bilayer graphene," *Nature* **574**, 653 (2019).
- <sup>8</sup> Y. Xie, B. Lian, B. Jäck, X. Liu, C.-L. Chiu, K. Watanabe, T. Taniguchi, B. A. Bernevig, and A. Yazdani, "Spectroscopic signatures of many-body correlations in magic-angle twisted bilayer graphene," *Nature* **572**, 101 (2019).
- <sup>9</sup> A. Kerelsky, L. J. McGilly, D. M. Kennes, L. Xian, M. Yankowitz, S. Chen, K. Watanabe, T. Taniguchi, J. Hone, C. Dean, A. Rubio, and A. N. Pasupathy, "Maximized electron interactions at the magic angle in twisted bilayer graphene," *Nature* **572**, 95 (2019).
- <sup>10</sup> Y. Jiang, X. Lai, K. Watanabe, T. Taniguchi, K. Haule, J. Mao, and E. Y. Andrei, "Charge order and broken rotational symmetry in magic-angle twisted bilayer graphene," *Nature* **573**, 91 (2019).
- <sup>11</sup> A. Uri, S. Grover, Y. Cao, J.A. Crosse, K. Bagani, D. Rodan-Legrain, Y. Myasoedov, K. Watanabe, T. Taniguchi, P. Moon, M. Koshino, P. Jarillo-Herrero, and E. Zeldov, "Mapping the twist-angle disorder and Landau levels in magic-angle graphene," *Nature* **581**, 47 (2020).
- <sup>12</sup> K. P. Nuckolls, M. Oh, D. Wong, B. Lian, K. Watanabe, T. Taniguchi, B. A. Bernevig, and A. Yazdani, "Strongly correlated Chern insulators in magic-angle twisted bilayer graphene," *Nature* **588**, 610 (2020).
- <sup>13</sup> E. Khalaf, A. J. Kruchkov, G. Tarnopolsky, and A. Vishwanath, "Magic angle hierarchy in twisted graphene multilayers," *Phys. Rev. B* **100**, 085109 (2019).
- <sup>14</sup> C. Mora, N. Regnault, and B. A. Bernevig, "Flatbands and Perfect Metal in Trilayer Moiré Graphene," *Phys. Rev. Lett.* **123**, 026402 (2019).
- <sup>15</sup> S. Carr, C. Li, Z. Zhu, E. Kaxiras, S. Sachdev, and A. Kruchkov, "Ultraheavy and Ultrarelativistic Dirac Quasiparticles in Sandwiched Graphenes," *Nano Lett.* **20**, 3030 (2020).
- <sup>16</sup> D. Călugăru, F. Xie, Z.-D. Song, B. Lian, N. Regnault, and B. A. Bernevig, "Twisted symmetric trilayer graphene: Single-particle and many-body Hamiltonians and hidden nonlocal symmetries of trilayer moiré systems with and without displacement field," *Phys. Rev. B* **103**, 195411 (2021).
- <sup>17</sup> V. T. Phong, P. A. Pantaleón, T. Cea, and F. Guinea, "Band structure and superconductivity in twisted trilayer graphene," *Phys. Rev. B* **104**, L121116 (2021).
- <sup>18</sup> J. Shin, B. L. Chittari, and J. Jung, "Stacking and gate-tunable topological flat bands, gaps, and anisotropic strip patterns in twisted trilayer graphene," *Phys. Rev. B* **104**, 045413 (2021).



- <sup>19</sup> Y. W. Choi and H. J. Choi, “Dichotomy of Electron-Phonon Coupling in Graphene Moiré Flat Bands,” *Phys. Rev. Lett.* **127**, 167001 (2021).
- <sup>20</sup> C. Lei, L. Linhart, W. Qin, F. Libisch, and A. H. MacDonald, “Mirror symmetry breaking and lateral stacking shifts in twisted trilayer graphene,” *Phys. Rev. B* **104**, 035139 (2021).
- <sup>21</sup> W. Qin and A. H. MacDonald, “In-Plane Critical Magnetic Fields in Magic-Angle Twisted Trilayer Graphene,” *Phys. Rev. Lett.* **127**, 097001 (2021).
- <sup>22</sup> Z. Wu, Z. Zhan, and S. Yuan, “Lattice relaxation, mirror symmetry and magnetic field effects on ultraflat bands in twisted trilayer graphene,” *Science China Physics, Mechanics & Astronomy* **64**, 267811 (2021).
- <sup>23</sup> A. Ramires and J. L. Lado, “Emulating Heavy Fermions in Twisted Trilayer Graphene,” *Phys. Rev. Lett.* **127**, 026401 (2021).
- <sup>24</sup> M. Christos, S. Sachdev, and M. S. Scheurer, “Correlated insulators, semimetals, and superconductivity in twisted trilayer graphene,” [arXiv:2106.02063](https://arxiv.org/abs/2106.02063).
- <sup>25</sup> A. Fischer, Z. A. H. Goodwin, A. A. Mostofi, J. Lischner, D. M. Kennes, and L. Klebl, “Unconventional superconductivity in magic-angle twisted trilayer graphene,” *npj Quantum Materials* **7**, 5 (2022).
- <sup>26</sup> Z. Zhu, S. Carr, D. Massatt, M. Lusk, and E. Kaxiras, “Twisted Trilayer Graphene: A Precisely Tunable Platform for Correlated Electrons,” *Phys. Rev. Lett.* **125**, 116404 (2020).
- <sup>27</sup> S. Dai, Y. Xiang, and D. J. Srolovitz, “Twisted Bilayer Graphene: Moiré with a Twist,” *Nano Lett.* **16**, 5923 (2016).
- <sup>28</sup> N. N. T. Nam and M. Koshino, “Lattice relaxation and energy band modulation in twisted bilayer graphene,” *Phys. Rev. B* **96**, 075311 (2017).
- <sup>29</sup> X. Lin, D. Liu, and D. Tománek, “Shear instability in twisted bilayer graphene,” *Phys. Rev. B* **98**, 195432 (2018).
- <sup>30</sup> H. Yoo, R. Engelke, S. Carr, S. Fang, K. Zhang, P. Cazeaux, S. H. Sung, R. Hovden, A. W. Tsen, T. Taniguchi, K. Watanabe, G.-C. Yi, M. Kim, M. Lusk, E. B. Tadmor, E. Kaxiras, and P. Kim, “Atomic and electronic reconstruction at the van der Waals interface in twisted bilayer graphene,” *Nat. Mater.* **18**, 448 (2019).
- <sup>31</sup> P. Lucignano, D. Alfè, V. Cataudella, D. Ninno, and G. Cantele, “Crucial role of atomic corrugation on the flat bands and energy gaps of twisted bilayer graphene at the magic angle  $\theta \sim 1.08^\circ$ ,” *Phys. Rev. B* **99**, 195419 (2019).
- <sup>32</sup> F. Guinea and N. R. Walet, “Continuum models for twisted bilayer graphene: Effect of lattice deformation and hopping parameters,” *Phys. Rev. B* **99**, 205134 (2019).
- <sup>33</sup> Y. W. Choi and H. J. Choi, “Intrinsic band gap and electrically tunable flat bands in twisted double bilayer graphene,” *Phys. Rev. B* **100**, 201402 (2019).
- <sup>34</sup> X. Lin, H. Zhu, and J. Ni, “Pressure-induced gap modulation and topological transitions in twisted bilayer and twisted double bilayer graphene,” *Phys. Rev. B* **101**, 155405 (2020).
- <sup>35</sup> S. Turkel, J. Swann, Z. Zhu, M. Christos, K. Watanabe, T. Taniguchi, S. Sachdev, M. S. Scheurer, E. Kaxiras, C. R. Dean, and A. N. Pasupathy, “Twistons in a Sea of Magic,” [arXiv:2109.12631](https://arxiv.org/abs/2109.12631).
- <sup>36</sup> Z. Zhu, P. Cazeaux, M. Lusk, and E. Kaxiras, “Modeling mechanical relaxation in incommensurate trilayer van der Waals heterostructures,” *Phys. Rev. B* **101**, 224107 (2020).
- <sup>37</sup> X. Zhang, K.-T. Tsai, Z. Zhu, W. Ren, Y. Luo, S. Carr, M. Lusk, E. Kaxiras, and K. Wang, “Correlated Insulating States and Transport Signature of Superconductivity in Twisted Trilayer Graphene Superlattices,” *Phys. Rev. Lett.* **127**, 166802 (2021).
- <sup>38</sup> A. L. Sharpe, E. J. Fox, A. W. Barnard, J. Finney, K. Watanabe, T. Taniguchi, M. A. Kastner, and D. Goldhaber-Gordon, “Emergent ferromagnetism near three-quarters filling in twisted bilayer graphene,” *Science* **365**, 605 (2019).
- <sup>39</sup> M. Serlin, C. L. Tschirhart, H. Polshyn, Y. Zhang, J. Zhu, K. Watanabe, T. Taniguchi, L. Balents, and A. F. Young, “Intrinsic quantized anomalous Hall effect in a moiré heterostructure,” *Science* **367**, 900 (2020).
- <sup>40</sup> S. Chatterjee, N. Bultinck, and M. P. Zaletel, “Symmetry breaking and skyrmionic transport in twisted bilayer graphene,” *Phys. Rev. B* **101**, 165141 (2020).
- <sup>41</sup> T. Cea, P. A. Pantaleón, and F. Guinea, “Band structure of twisted bilayer graphene on hexagonal boron nitride,” *Phys. Rev. B* **102**, 155136 (2020).
- <sup>42</sup> X. Lin, K. Su, and J. Ni, “Misalignment instability in magic-angle twisted bilayer graphene on hexagonal boron nitride,” *2D Mater.* **8**, 025025 (2021).
- <sup>43</sup> J. Shi, J. Zhu, and A. H. MacDonald, “Moiré commensurability and the quantum anomalous Hall effect in twisted bilayer graphene on hexagonal boron nitride,” *Phys. Rev. B* **103**, 075122 (2021).
- <sup>44</sup> D. Mao and T. Senthil, “Quasiperiodicity, band topology, and moiré graphene,” *Phys. Rev. B* **103**, 115110 (2021).
- <sup>45</sup> J. M. B. Lopes dos Santos, N. M. R. Peres, and A. H. Castro Neto, “Graphene Bilayer with a Twist: Electronic Structure,” *Phys. Rev. Lett.* **99**, 256802 (2007).
- <sup>46</sup> E. J. Mele, “Commensuration and interlayer coherence in twisted bilayer graphene,” *Phys. Rev. B* **81**, 161405 (2010).
- <sup>47</sup> G. Li, A. Luican, J. M. B. Lopes dos Santos, A. H. Castro Neto, A. Reina, J. Kong, and E. Y. Andrei, “Observation of Van Hove singularities in twisted graphene layers,” *Nat. Phys.* **6**, 109 (2010).
- <sup>48</sup> J. M. B. Lopes dos Santos, N. M. R. Peres, and A. H. Castro Neto, “Continuum model of the twisted graphene bilayer,” *Phys. Rev. B* **86**, 155449 (2012).
- <sup>49</sup> J. S. Alden, A. W. Tsen, P. Y. Huang, R. Hovden, L. Brown, J. Park, D. A. Muller, and P. L. McEuen, “Strain solitons and topological defects in bilayer graphene,” *Proc. Natl. Acad. Sci. U.S.A.* **110**, 11256 (2013).
- <sup>50</sup> C. R. Woods, L. Britnell, A. Eckmann, R. S. Ma, J. C. Lu, H. M. Guo, X. Lin, G. L. Yu, Y. Cao, R. V. Gorbachev, A. V. Kretinin, J. Park, L. A. Ponomarenko, M. I. Katsnelson, Y. N. Gornostyrev, K. Watanabe, T. Taniguchi, C. Casiraghi, H.-J. Gao, A. K. Geim, and K. S. Novoselov, “Commensurate-incommensurate transition in graphene on hexagonal boron nitride,” *Nat. Phys.* **10**, 451 (2014).
- <sup>51</sup> K. Uchida, S. Furuya, J.-I. Iwata, and A. Oshiyama, “Atomic corrugation and electron localization due to Moiré patterns in twisted bilayer graphenes,” *Phys. Rev. B* **90**, 155451 (2014).
- <sup>52</sup> P. San-Jose, A. Gutiérrez-Rubio, M. Sturla, and F. Guinea, “Electronic structure of spontaneously strained graphene on hexagonal boron nitride,” *Phys. Rev. B* **90**, 115152 (2014).
- <sup>53</sup> P. San-Jose, A. Gutiérrez-Rubio, M. Sturla, and F. Guinea, “Spontaneous strains and gap in graphene on boron nitride,” *Phys. Rev. B* **90**, 075428 (2014).
- <sup>54</sup> G. J. Slotman, M. M. van Wijk, P.-L. Zhao, A. Fasolino,

- M. I. Katsnelson, and S. J. Yuan, “Effect of Structural Relaxation on the Electronic Structure of Graphene on Hexagonal Boron Nitride,” *Phys. Rev. Lett.* **115**, 186801 (2015).
- <sup>55</sup> J. Jung, A. M. DaSilva, A. H. MacDonald, and S. Adam, “Origin of band gaps in graphene on hexagonal boron nitride,” *Nat. Commun.* **6**, 6308 (2015).
- <sup>56</sup> M. M. van Wijk, A. Schuring, M. I. Katsnelson, and A. Fasolino, “Relaxation of Moiré patterns for slightly misaligned identical lattices: graphene on graphite,” *2D Mater.* **2**, 034010 (2015).
- <sup>57</sup> S. K. Jain, V. Juričić, and G. T. Barkema, “Structure of twisted and buckled bilayer graphene,” *2D Mater.* **4**, 015018 (2017).
- <sup>58</sup> J. Jung, E. Laksono, A. M. DaSilva, A. H. MacDonald, M. Mucha-Kruczyński, and S. Adam, “Moiré band model and band gaps of graphene on hexagonal boron nitride,” *Phys. Rev. B* **96**, 085442 (2017).
- <sup>59</sup> F. Gargiulo and O. V. Yazyev, “Structural and electronic transformation in low-angle twisted bilayer graphene,” *2D Mater.* **5**, 015019 (2018).
- <sup>60</sup> S. Carr, D. Massatt, S. B. Torrisi, P. Cazeaux, M. Lusk, and E. Kaxiras, “Relaxation and domain formation in incommensurate two-dimensional heterostructures,” *Phys. Rev. B* **98**, 224102 (2018).
- <sup>61</sup> J.-B. Qiao, L.-J. Yin, and L. He, “Twisted graphene bilayer around the first magic angle engineered by heteros-train,” *Phys. Rev. B* **98**, 235402 (2018).
- <sup>62</sup> X. Lin and J. Ni, “Effective lattice model of graphene moiré superlattices on hexagonal boron nitride,” *Phys. Rev. B* **100**, 195413 (2019).
- <sup>63</sup> Y.-W. Liu, Y. Su, X.-F. Zhou, L.-J. Yin, C. Yan, S.-Y. Li, W. Yan, S. Han, Z.-Q. Fu, Y. Zhang, Q. Yang, Y.-N. Ren, and L. He, “Tunable Lattice Reconstruction, Triangular Network of Chiral One-Dimensional States, and Bandwidth of Flat Bands in Magic Angle Twisted Bilayer Graphene,” *Phys. Rev. Lett.* **125**, 236102 (2020).
- <sup>64</sup> D. Halbertal, N. R. Finney, S. S. Sunku, A. Kerelsky, C. Rubio-Verdú, S. Shabani, L. Xian, S. Carr, S. Chen, C. Zhang, L. Wang, D. Gonzalez-Acevedo, A. S. McLeod, D. Rhodes, K. Watanabe, T. Taniguchi, E. Kaxiras, C. R. Dean, J. C. Hone, A. N. Pasupathy, D. M. Kennes, A. Rubio, and D. N. Basov, “Moiré metrology of energy landscapes in van der Waals heterostructures,” *Nat. Commun.* **12**, 242 (2021).
- <sup>65</sup> A. C. Gadelha, D. A. A. Oehlberg, C. Rabelo, E. G. S. Neto, T. L. Vasconcelos, J. L. Campos, J. S. Lemos, V. Ornelas, D. Miranda, R. Nadas, F. C. Santana, K. Watanabe, T. Taniguchi, B. van Troeye, M. Lamparski, V. Meunier, V.-H. Nguyen, D. Paszko, J.-C. Charlier, L. C. Campos, L. G. Cançado, G. Medeiros-Ribeiro, and A. Jorio, “Localization of lattice dynamics in low-angle twisted bilayer graphene,” *Nature* **590**, 405 (2021).
- <sup>66</sup> X. Lin, H. Zhu, and J. Ni, “Emergence of intrinsically isolated flat bands and their topology in fully relaxed twisted multilayer graphene,” *Phys. Rev. B* **104**, 125421 (2021).
- <sup>67</sup> L. J. McGilly, A. Kerelsky, N. R. Finney, K. Shapovalov, E.-M. Shih, A. Ghiotto, Y. Zeng, S. L. Moore, W. Wu, Y. Bai, K. Watanabe, T. Taniguchi, M. Stengel, L. Zhou, J. Hone, X. Zhu, D. N. Basov, C. Dean, C. E. Dreyer, and A. N. Pasupathy, “Visualization of moiré superlattices,” *Nat. Nanotechnol.* **15**, 580 (2020).
- <sup>68</sup> Y. Li, X. Wang, D. Tang, X. Wang, K. Watanabe, T. Taniguchi, D. R. Gamelin, D. H. Cobden, M. Yankowitz, X. Xu, and J. Li, “Unraveling intrinsic flexoelectricity in twisted double bilayer graphene,” [arXiv:2104.02401](https://arxiv.org/abs/2104.02401).